Malaysian Journal Of Civil Engineering

Full Paper

VALIDATION AND PARAMETRIC STUDY OF LEAN DUPLEX STAINLESS STEEL HOLLOW SECTION STUB COLUMNS BY FINITE ELEMENT ANALYSIS

Article history
Received
29 September 2023
Received in revised form
06 May 2024
Accepted
03 Jun 2024
Published online
01 August 2024

Din Mohammad Jahed, Md. Istiaque Ahmed, Md. Sifatul Islam, Fatema-Tuz-Zahura*

Department of Civil Engineering, Ahsanullah University of Science and Technology, Bangladesh

*Corresponding author
fatema.ce@aust.edu

Graphical abstract

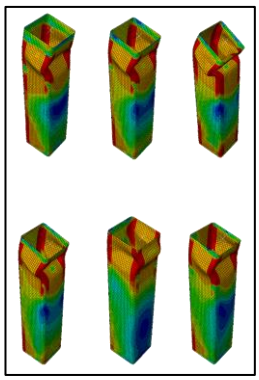

Abstract

In this research, a parametric study was conducted on square hollow sections (SHS) and rectangular hollow sections (RHS) columns made of a lean duplex stainless steel (LDSS) grade, namely EN 1.4162. The aim was to determine structural response data due to variations of different design parameters, which is vital in designing structural members. Finite element modeling was utilized for this and the validity of the models was confirmed by comparing them with existing experimental test data. Thickness, corner radius, load eccentricity and slenderness ratio were taken as the varying parameters to study. A total of 32 columns were modeled to study with five variations for each parameter, making a total of 160 variations. For each variation, the ultimate load and the corresponding end shortening were recorded. Each parameter has some effects on ultimate load or end shortening or both except corner radius, which has no significant effect. To visualize the effect of a parameter, a trend line equation was developed by plotting the average result of all column models for each variation of that particular parameter. A linear increase in ultimate load and end shortening can be observed with an increase in column thickness, while opposite trends were witnessed with load eccentricity. Though a linear rise in end shortening was caused by the slenderness ratio, no significant change was seen in the ultimate load of the columns. The mathematical equations presented can be employed to forecast the maximum load-bearing capacity and the associated amount of end shortening when designing structural hollow sections made of LDSS.

Keywords: Parametric study, finite element analysis, stainless steel, lean duplex stainless steel, hollow column

1.0 INTRODUCTION

Stainless steels come in a wide range of grades depending on the proportion of Carbon and other alloying materials. Duplex stainless steel, one of the steel grades, has recently received a lot of attention due to its higher strength than austenitic steel and better corrosion resistance than other steel grades [1]. Duplex stainless steel usually contains 8 to 15% nickel by weight, which results in more strength than austenitic stainless steel. However, the nickel content is also responsible for high manufacturing cost, so to minimize the initial cost, Lean Duplex Stainless Steel (LDSS) was introduced, containing approximately 1.5% nickel [2]. Due to the low alloy adjustment factor, it is more affordable than other grades of stainless steel. The use of LDSS is increasing steadily because of its excellent characteristics. The new Doha airport's roof in Qatar; the continuous sulfate pulp digester and impregnation tower, Sweden; Heathrow airport, UK are great examples. Hollow structural sections are widely used because they are lightweight and aesthetically pleasing. The growing popularity of LDSS prompted early researchers to conduct studies on its properties, behavior and applications. Both experimental and numerical studies have been conducted on various shapes of LDSS by other researchers [3-13], such as hollow square, circular, rectangular, oval sections as well as I-beams and columns.

The study opted for rectangular and square hollow sections because of their greater accessibility and widespread application in steel structures [14].This research was carried out in order to observe how the characteristics, such as ultimate load (F_u) and deformation (d_U) , vary due to changes in the physical parameters of the rectangular and square hollow columns made of LDSS. Since these large numbers of different models (32 models and a total of 160 variations in parameters) were not feasible to test in the laboratory due to limited resources and time, the study was carried out using Finite Element Analysis (FEA). The finite element models needed to be validated against experimental test data to get reliable and accurate results. The experimental test data from article [12] was selected to verify the accuracy of the finite element models. Although similar studies were carried out previously, they studied different parameters, materials and shapes [15-19]. This research was essential because there is a lack of trustworthy data from a comprehensive analysis that incorporates these specific parameters for hollow columns of this nature. In addition, the relationship between each parameter and the corresponding F_u and d_U was determined and expressed by equations.

2.0 FINITE ELEMENT MODELING

2.1 General

Finite element modeling of the LDSS hollow sections was done in a finite element package. Different geometric aspects of the column section, i.e., thickness (t), the radius of curvature (r_i), slenderness ratio and load eccentricity, were changed in order to see its effect. These finite element analyses were performed considering only the local geometric imperfection. First, these FE (finite element) models were validated by using the experimental study data obtained from an experiment on LDSS hollow section performed by Theofanous et al [12]. Later, these validated FE models were used for parametric study. The major modeling parameters adopted in this study are described in the subsequent sections.

2.2 Material Modeling

A stainless-steel column can be made in two distinct manners: one with a curved corner area and the other with a flat corner area. The curved corner areas of stainless steel exhibit greater strength compared to the flat corner areas [20]. For this reason, columns with a curved corner were used in this study. Equation (1) & Equation (2) were utilized in this work to predict the stress-strain behavior accurately.

$$\varepsilon = \frac{\sigma_{0.2}}{E_0} + 0.002\left(\frac{\sigma}{\sigma_{0.2}}\right)^n \quad for\ \sigma \leq \sigma_{0.2} \tag{1}$$

$$\varepsilon = \frac{(\sigma-\sigma_{0.2})}{E_{0.2}} + \left(\varepsilon_{t1.0} - \varepsilon_{t0.2} - \frac{\sigma_{1.0}-\sigma_{0.2}}{E_{0.2}}\right)\left(\frac{\sigma-\sigma_{0.2}}{\sigma_{1.0}-\sigma_{0.2}}\right)^{n'_{0.2,1.0}} + \varepsilon_{t0.2} \tag{2}$$

$for\ \sigma > \sigma_{0.2}$

Where, σ = Engineering stress

ε = Engineering strain

$\sigma_{0.2}$ = 0.2% proof stresses

$\sigma_{1.0}$ = 1% proof stresses

$\varepsilon_{t0.2}$ = Total strains corresponding to $\sigma_{0.2}$

$\varepsilon_{t1.0}$ = Total strains corresponding to $\sigma_{1.0}$

E_0 = Material's Young's modulus

$E_{0.2}$ = Material's tangent modulus at $\sigma_{0.2}$

n = and $n'_{0.2,1.0}$ Used as the exponential constants to appropriately consider the material nonlinearity.

According to Ramberg et al. [21], Equation (1) provides a reliable prediction of the stress-strain curve when the stresses are below the 0.2% proof stress ($\sigma_{0.2}$). On the other hand, Gardner et al. [20] suggested that Equation (2) yields more accurate stress-strain curves for stresses above the 0.2% proof stress ($\sigma_{0.2}$).

$$\varepsilon_{true} = ln\,(1 + \varepsilon_{engineering}) \quad (3)$$

$$\sigma_{true} = \sigma_{engineering}\,(1 + \varepsilon_{engineering}) \quad (4)$$

Where, $\sigma_{engineering}$ is the engineering stress

$\varepsilon_{engineering}$ is the engineering strain

σ_{true} is the true stress

ε_{true} is the true strain

These two equations (Equation (1) and Equation (2)) mentioned above provide engineering stress and strain. To utilize engineering stress and strain in the finite element package, two additional equations, Equations (3) and Equation (4), were employed to convert them into true stress and strain. This conversion was necessary because finite element packages exclusively utilize true stress-strain values.

The material properties of a square column are categorized into three sections based on their behavior: tensile flat, compressive flat, and tensile corner. Table 1, Table 2, and Table 3 present the respective properties for each section, which obtained from the experimental study conducted by Theofanous et al. [12]. Table 1, Table 2 & Table 3 display various properties of the above-mentioned material section utilized in this study, including Young's modulus (*E*), 0.2% and 1% proof stresses ($\sigma_{0.2}$ and $\sigma_{1.0}$ respectively). Also, the ultimate tensile stress σ_u and the plastic strain at the fracture ε_f of the material are shown in the tables. Table 1, Table 2 & Table 3 also include the values of strain hardening exponent n and $n'_{0.2,1.0}$ used in the compound Ramberg-Osgood (*R-O*) material model [15, 22-24].

Table 1: Material properties (Tensile flat) [12]

Cross-section	*E* (N/mm²)	$\sigma_{0.2}$ (N/mm²)	$\sigma_{1.0}$ (N/mm²)	σ_u (N/mm²)	ε_f (%)	Compound *R–O* coefficients	
						n	$n'_{0.2,1.0}$
SHS 100 × 100 × 4	198 800	586	632	761	47	9.0	2.8

Table 2: Material properties (Compressive flat) [12]

Cross-section	*E* (N/mm²)	$\sigma_{0.2}$ (N/mm²)	$\sigma_{1.0}$ (N/mm²)	Compound *R–O* coefficients	
				n	$n'_{0.2,1.0}$
SHS 100 × 100 × 4	198 200	560	642	8.3	2.6

Table 3: Material properties (Tensile Corner) [12]

Cross-section	*E* (N/mm²)	$\sigma_{0.2}$ (N/mm²)	$\sigma_{1.0}$ (N/mm²)	σ_u (N/mm²)	ε_f (%)	Compound *R–O* coefficients	
						n	$n'_{0.2,1.0}$
SHS 100 × 100 × 4	206 000	811	912	917	32	6.3	4.1

Table 4: Measured dimensions of stub columns [12]

Specimen	*L* (mm)	*B* (mm)	*H* (mm)	*t* (mm)	r_i (mm)	*A* (mm²)	w_0 (mm)
SHS 100x100x4-SC1	400	101	102	3.93	3.8	1495.2	0.071
SHS 100x100x4-SC2	400	102	103	3.97	3.9	1524.7	0.071
SHS 80x80x4-SC1	319.7	80	80.5	3.88	3.8	1147.4	0.08
SHS 80x80x4-SC2	332.2	80	80	3.81	3.6	1125	0.08
SHS 60x60x3-SC1	239.8	60	60	3.09	2.3	683	0.062

SHS 60x60x3-SC2	240	60	60	3.17	2.1	700.4	0.062
RHS 80x40x4-SC1	239.9	39	79.5	3.76	3.5	799.8	0.058
RHS 80x40x4-SC2	237.8	39.6	79.5	3.81	4.3	808.8	0.058

Table 4 shows different parameters of a specimen, where the length is denoted as *L*, whereas *B* and *H* are the widths of the section, while *t* and r_i are the corresponding thickness and corner radius, at last, *A* and ω_0 are the cross-sectional area and local geometric imperfection, respectively. Here, mainly four different types of columns are used; three of them are Square Hollow Section (SHS) columns and one of them is a Rectangular Hollow Section (RHS) column. Each of the column types has two specimens (*i.e*, SC1 and SC2), which makes eight specimens in total. As we utilized Article [12] for modeling data and for validation of the models, we followed the same specimen naming process used in that article. Specimen name SHS 100x100x4 SC-1 denotes the first specimen (SC-1) of hollow Square Section (SHS) with 100 mm width (100x100) and 400 mm long.

2.3 Geometry and Boundary Condition

The stub columns modelled in this study were fixed-ended. There have been some previous studies [12, 17, 18, 22] on modeling fixed-ended columns that were followed in this study. Material properties for the hollow column sections are discretely assigned in the finite element model, as shown in Figure 1 [12, 20]. While Figure 2 illustrates the boundary condition of the LDSS hollow column section. A wide variety of thicknesses, corner radius, length and cross-sections were used in this study to observe the load-carrying capacity of the column. Here, both ends of the column are tied to the corresponding reference points (RP), these reference points are in the same plane as the top and bottom edges. Then, the boundary condition is applied to these reference points. At the lower end of the column, all degrees of freedom are constrained. Whereas at the upper end, where the load is applied, is also constrained in all degrees of freedom except for the vertical displacement. Unit vertical displacement was applied at the loading end (RP-2) to obtain the eigenmodes.

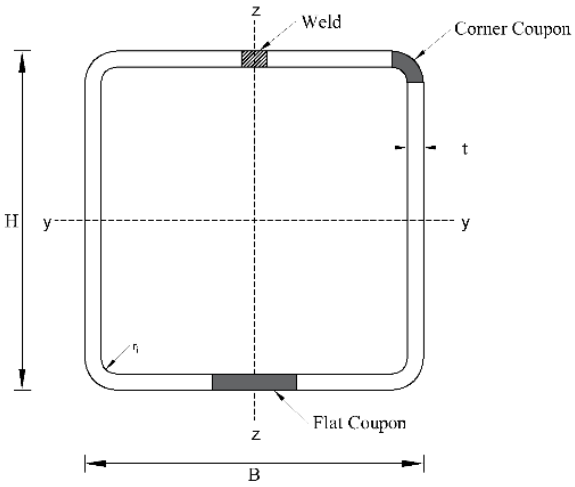

Figure 1 Cross-section of the LDSS hollow stub column

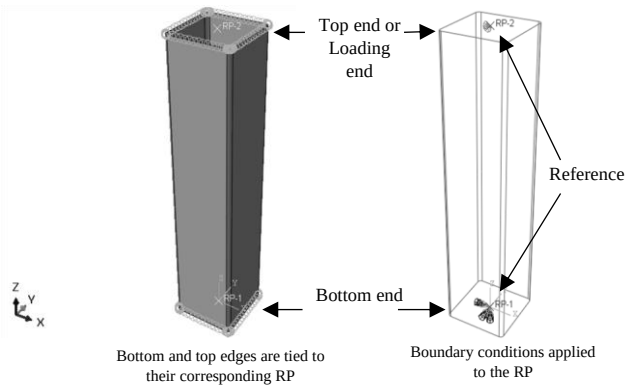

Figure 2 Typical Boundary Condition of LDSS Hollow Column

2.4 Element Type

Among tons of element types available in the finite element package, there are two types of shell elements that are generally used for stainless steel components: general-purpose S4R [25, 26] or thin shell S9R5 [20, 23]. Though these two elements are hard to distinguish, the load-deformation curves for S9R5 tend to become relatively flat at the peak load (F_u) , which makes it difficult to predict the deformation at the ultimate load (d_U) [27].So, in this study, S4R element is used.

2.5 Finite Element Mesh

Two distinct mesh sizes were employed to determine which one would produce a more accurate load-deformation curve prediction. Figure 3(a) & Figure 3(b) show fine mesh and coarse mesh, respectively. For fine mesh, its size was determined by the corresponding material thickness (*t*), which varies from 3.09 to 3.97 mm. Whereas for the course mesh, its size was twice the corresponding material thickness (*t*), and its sizes varied from 6.18 to 7.94 mm. A comparison of the ultimate load capacity (F_u) and the deformation at maximum loading (d_U) is shown in Table 5 for the aforementioned mesh sizes, along with test results obtained by Theofanous et al. [12].

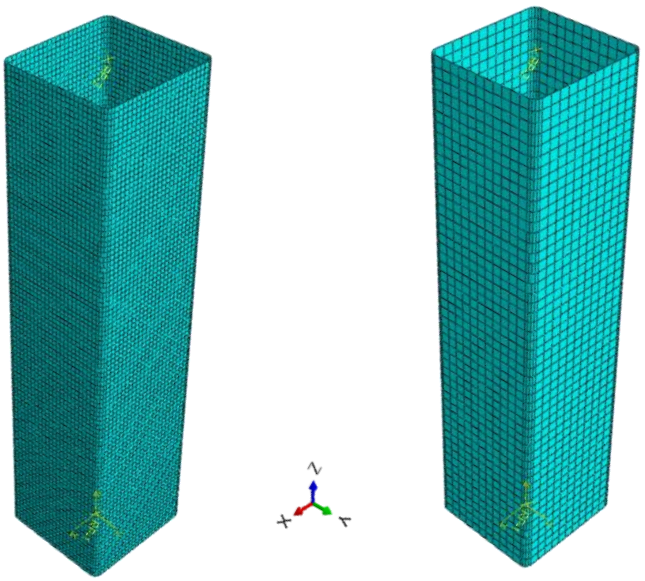

(a) Fine Mesh Size = t

(b) Coarse Mesh Size = 2t

Figure 3 100x100x4-SC1 Stub Column with Different Mesh Sizes

Table 5 Findings of the FE analyses of stub columns using certain meshes to produce load-deformation ratios

	Designation	Test Results		Mesh Size = 2*t*		Mesh Size = *t*	
		F_u (KN)	δ_u (mm)	FE F_u/ Test F_u	FE δ_u/ Test δ_u	FE F_u/ Test F_u	FE δ_u/ Test δ_u
SHS	100x100x4-SC1	1022	3.63	0.942	0.683	**0.950**	**0.749**
	100x100x4-SC2	1037	4.01	0.929	0.646	**0.956**	**0.679**
	80x80x4-SC1	923	4.13	1.028	**0.987**	**1.024**	0.968
	80x80x4-SC2	915	3.88	1.009	1.049	**1.006**	**1.035**
	60x60x3-SC1	613	4.09	1.017	**0.781**	**1.014**	0.768
	60x60x3-SC2	616	3.69	1.049	**0.986**	**1.045**	0.903
RHS	80x40x4-SC1	709	4.33	0.961	0.804	**0.962**	**0.821**
	80x40x4-SC2	710	4.12	**0.978**	0.828	0.976	**0.837**
All Sections		Average		0.989	0.845	**0.992**	**0.845**
		SD		0.043	0.148	**0.035**	**0.118**
		COV		0.044	0.175	**0.036**	**0.140**
		Percent Error (%)		3.78%	22.75%	**3.13%**	**21.24%**

2.6 Extent of Corner Enhancement

The material properties of the corner coupon area, as shown in Figure 1, were extended beyond the corner portion in order to achieve realistic results [20]. Previous studies done by Karren et al. [26] showed that for the carbon steel section, the increased yield portion must go all the way to thickness *t*. Whereas Abdel et al. [28] showed that the distance should be $0.5\pi r_i$ beyond the corner. Figure 4 shows three different corner enhancements and Table 6 shows a comparison of ultimate load carrying capacities (F_u) and deformation at ultimate load (d_U) of these three different corner enhancements with respect to the test findings by Theofanous et al. [12]. Here, in this instance, *2t* enhancement of the corner region showed more accurate results than others. For the further parametric study, *2t* corner enhancement was chosen.

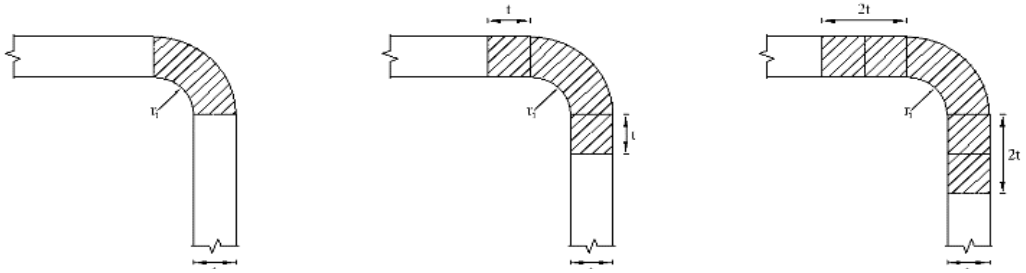

(a) Corner region only (b) Corner region plus t (c) Corner region plus 2t

Figure 4 Different scenarios were examined in order to assess the extent of corner enhancement

Table 6 Load deformation result after applying different corner enhancement

	Designation	Test Results		Corner Extended 2*t*		Corner Extended *t*		Without Corner Extension	
		F_u (KN)	δ_u (mm)	FE F_u/ Test F_u	FE δ_u/ Test δ_u	FE F_u/ Test F_u	FE δ_u/ Test δ_u	FE F_u/ Test F_u	FE δ_u/ Test δ_u
SHS	100x100x4-SC1	1022	3.63	**0.950**	0.749	0.919	0.745	0.888	**0.762**
	100x100x4-SC2	1037	4.01	**0.956**	**0.730**	0.927	0.718	0.893	0.691
	80x80x4-SC1	923	4.13	1.024	**0.968**	**1.001**	0.959	0.974	0.955
	80x80x4-SC2	915	3.88	**1.006**	1.035	0.983	1.031	0.960	**1.020**
	60x60x3-SC1	613	4.09	**1.014**	**0.810**	0.994	0.781	0.968	0.779

	60x60x3-SC2	616	3.69	1.045	**0.903**	1.022	0.901	**0.999**	0.900
RHS	80x40x4-SC1	709	4.33	**0.962**	**0.821**	0.925	0.812	0.887	0.791
	80x40x4-SC2	710	4.12	**0.976**	**0.837**	0.940	0.836	0.902	0.818
All Sections		Average		**0.992**	**0.856**	0.964	0.848	0.934	0.839
		SD		**0.035**	**0.105**	0.041	0.108	0.046	0.110
		COV		**0.036**	**0.123**	0.042	0.128	0.049	0.131
		Percent Error (%)		**3.13%**	**19.10%**	4.45%	20.32%	7.31%	21.35%

2.7 Local Geometric Imperfection

In this study, linear elastic eigenvalue buckling analysis was carried out to obtain the buckling mode shape of columns by using the Lanczos method since eigenvalue buckling is generally used to estimate the critical buckling load of stiff structures. In order to capture the accurate load-deformation response, the Modified Riks method [29, 30] was used. In a linear elastic eigenanalysis, the least local buckling mode is often the first eigenvalue. This eigenvalue was employed to perturb the geometry of the columns and it is then scaled with a local imperfection amplitude of 1% of the plate thickness, which is *t/100* as suggested by the literature [17, 19, 31]. A typical example of various elastic buckling mode shapes obtained from different eigenmodes for different shapes of columns is shown in Figure 5.

3.0 VALIDATION OF FINITE ELEMENT MODEL

To illustrate the reliability and accuracy of the method used for Finite Element modeling, it is necessary to be validated compared with the reliable results obtained from experimental tests. For this study, experimental data reported by Theofanous et al. [12] is adopted. Eight LDSS hollow section stub columns were reported by Theofanous et al. [12]. Each of them was modelled for Finite Element Analysis using the geometric data given in Table 4. The models were examined in relation to the relevant experimental findings, which are shown in Table 7 & Figure 6. Based on the validation results, it can be concluded that the Finite Element Modeling approach used here is capable of generating results that are comparable to those obtained from experimental tests.

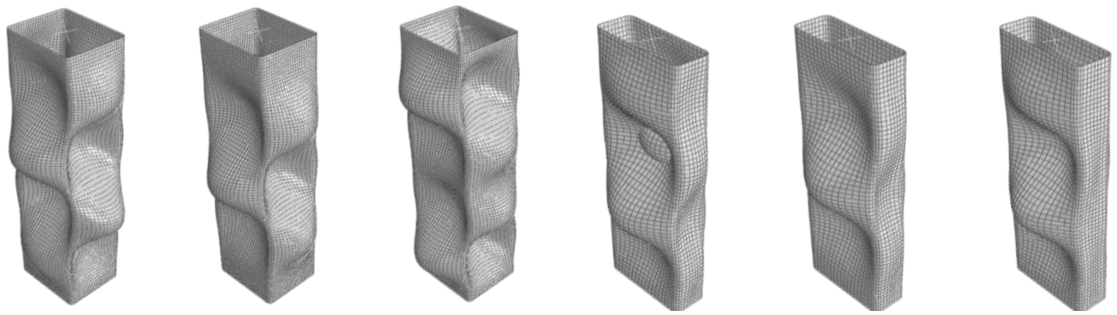

(a) SHS Eigen mode 1 (b) SHS Eigen mode 2 (c) SHS Eigen mode 3 (d) RHS Eigen mode 1 (e) RHS Eigen mode 2 (f) RHS Eigen mode 3

Figure 5 Different Eigenmode Shapes for Square and Rectangular Hollow Column Sections

Table 7 Comparison of FE results with test results

Designation		Test Results		*t*/100	
		F_u (KN)	δ_u (mm)	FE F_u/ Test F_u	FE δ_u/ Test δ_u
SHS	100x100x4-SC1	1022	3.63	**0.950**	**0.749**
	100x100x4-SC2	1037	4.01	**0.956**	**0.679**
	80x80x4-SC1	923	4.13	**1.024**	**0.968**
	80x80x4-SC2	915	3.88	**1.006**	**1.035**
	60x60x3-SC1	613	4.09	**1.014**	**0.768**
	60x60x3-SC2	616	3.69	**1.045**	**0.903**
RHS	80x40x4-SC1	709	4.33	**0.962**	**0.821**
	80x40x4-SC2	710	4.12	**0.976**	**0.837**
All Sections		Average		**0.992**	**0.845**
		SD		**0.035**	**0.118**
		COV		**0.036**	**0.140**
		Percent Error (%)		**3.13%**	**21.25%**

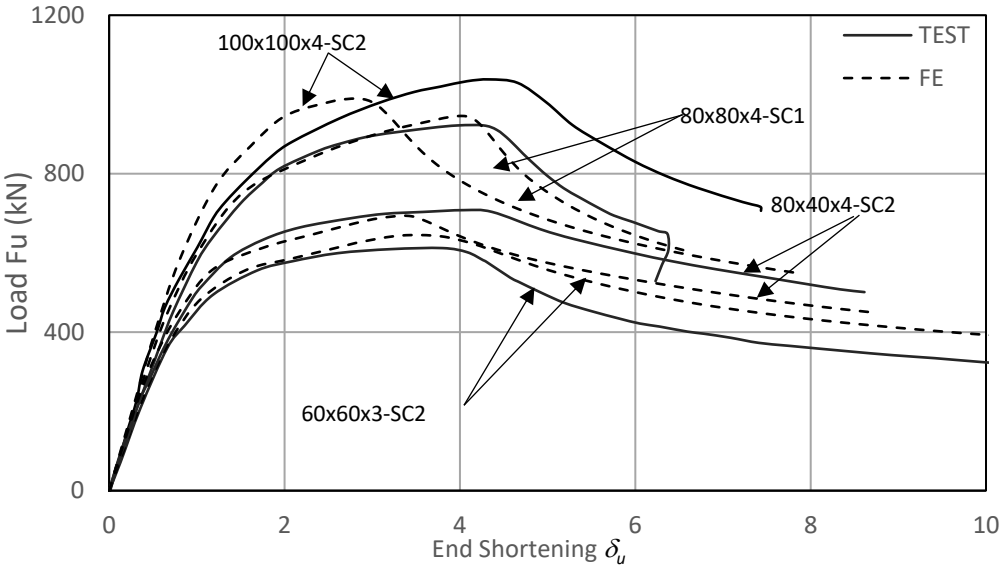

Figure 6 Experimental and numerical load–lateral displacement cures for different columns

4.0 PARAMETRIC STUDY

4.1 General

A parametric study of 32 models was conducted in order to study the variations of the outcome due to the changes in the modeling parameters. The parameters considered for the parametric study are thickness, corner radius, load eccentricity and column slenderness. Although models with different values of other parameters, such as mesh size, local geometric imperfection and extension of the corner into the flat portion, are studied as a part of the validation of finite element modeling, they were excluded from the parametric study. This is because the best values of these parameters were suggested in various previous studies [12, 16, 18, 30], and similar values were also found to provide the best outcome while validating the FE models in this study. Several values for each parameter were taken in this study to understand the trends and how the ultimate load-carrying capacity of the columns is affected by these parameters.

4.2 Column Thickness

A total of five different values for thickness were taken, ranging from *0.5t* to *2t*, where *t* is the thickness of the tested specimen. Figure 7 shows cross-sections of all the different thicknesses used in this study. The corner enhancement by *2t* for all columns is also shown in Figure 7. The behavior of the specimens was recorded and presented in Table 8 and Figure 8 & Figure 9.

Figure 7 A comparison of different thickness applied to a column

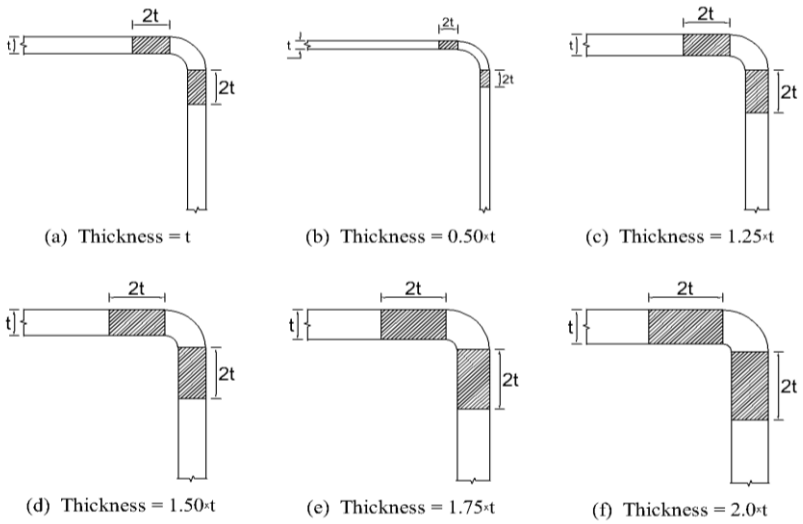

Table 8 Results (Load & deformation) obtained from the Parametric Study of stub columns of various thickness

Designation	Test Results		Thickness = $t/2$		Thickness = 1.25t		Thickness = 1.5t		Thickness = 1.75t		Thickness = 2t	
	F_u	d_U	FE F_u	FE d_U	FE F_u	FE d_U	FE F_u	FE d_U	FE F_u	FE d_U	FE F_u	FE d_U
	(KN)	(mm)	(KN)	(mm)	(KN)	(mm)	(KN)	(mm)	(KN)	(mm)	(KN)	(mm)
100x100x4-SC1	1022	3.63	271	1.76	1369	5.24	1663	6.14	1947	7.37	2232	9.03
100x100x4-SC2	1037	4.01	277	1.77	1399	5.49	1697	6.23	1986	7.07	2277	8.91
80x80x4-SC1	923	4.13	259	1.04	1216	5.06	1465	6.19	1717	8.67	1971	10.89
80x80x4-SC2	915	3.88	248	1.07	1191	5.37	1434	6.71	1681	8.64	1927	9.88
60x60x3-SC1	613	4.09	182	0.93	793	4.40	956	5.12	1121	7.46	1287	9.00
60x60x3-SC2	616	3.69	192	0.89	814	4.32	982	5.64	1151	7.69	1322	9.45
80x40x4-SC1	709	4.33	231	1.36	860	5.10	1044	7.80	1235	11.79	1415	12.97
80x40x4-SC2	710	4.12	244	1.21	877	4.99	1066	8.34	1261	12.07	1446	13.56

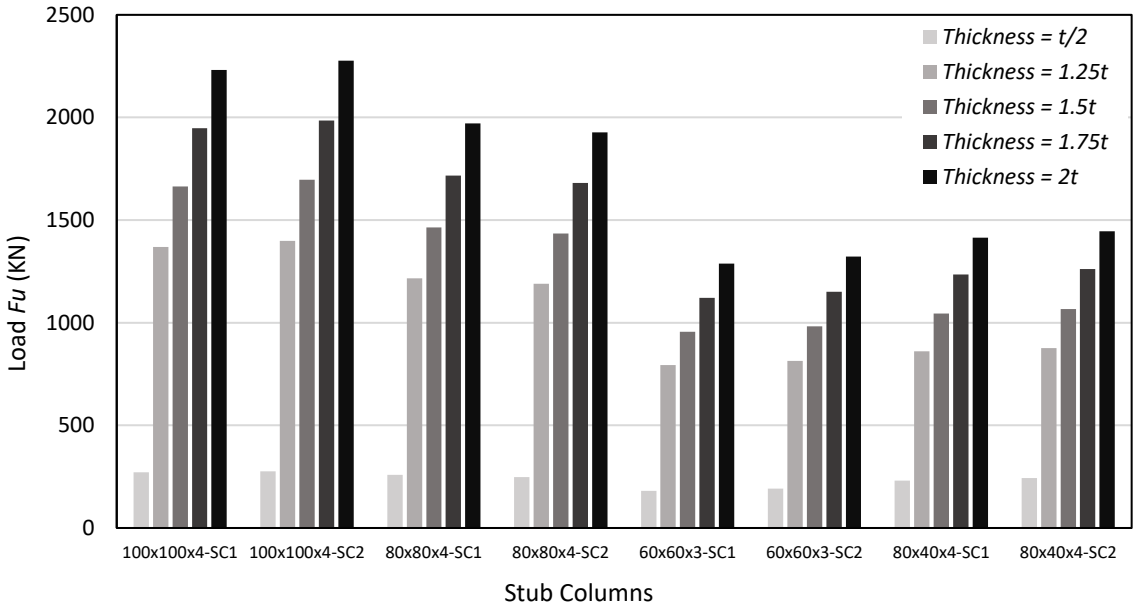

Figure 8 Maximum Load obtained with varying thickness for different columns

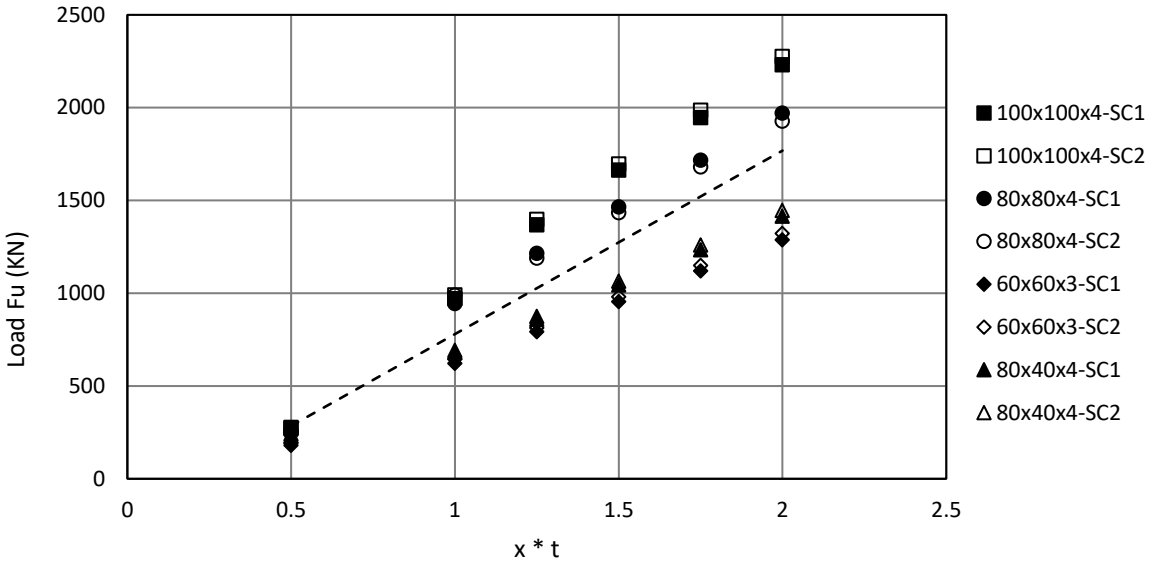

Figure 9 Ultimate load carried by the stub columns at different thickness

4.3 Corner Radius

The corner of the hollow columns can have different radius when the flat sheets are bent to make a hollow column. Five different corner radius were considered for the parametric study to see how it affects the capacity of the columns, Figure 10 shows cross-sections of different corner radius used for this study. The effects of the corner radius observed are presented in tabulated form in Table 9 as well as in graphical form in Figure 11.

Table 9 Findings (Load & deformation) gathered from the Parametric Study of stub columns with various corner radius

Designation	Test Results		Radius, *ri* = *L/B*		Radius, *ri* = *B/10*		Radius, *ri* = *t*		Radius, *ri* = *2t*		Radius, *ri* = *3t*	
	F_u	d_U	FE F_u	FE d_U	FE F_u	FE d_U	F_u	d_U	FE F_u	FE d_U	FE F_u	FE d_U
	(KN)	(mm)	(KN)	(mm)	(KN)	(mm)	(KN)	(mm)	(KN)	(mm)	(KN)	(mm)
100x100x4-SC1	1022	3.63	973	2.72	998	3.11	975	2.76	988	3.07	1012	3.41
100x100x4-SC2	1037	4.01	991	2.72	1000	2.84	991	2.72	1008	3.08	1032	3.41
80x80x4-SC1	923	4.13	948	4.08	922	4.05	949	4.07	943	4.02	954	4.58
80x80x4-SC2	915	3.88	921	4.03	920	4.08	921	4.12	921	4.11	932	4.59
60x60x3-SC1	613	4.09	622	3.26	623	3.46	623	3.27	622	3.48	624	3.81
60x60x3-SC2	616	3.69	643	3.41	642	3.59	643	3.37	641	3.63	641	3.78
80x40x4-SC1	709	4.33	682	3.44	681	3.35	681	3.34	683	3.42	674	3.41
80x40x4-SC2	710	4.12	695	3.36	695	3.48	693	3.33	694	3.25	687	3.40

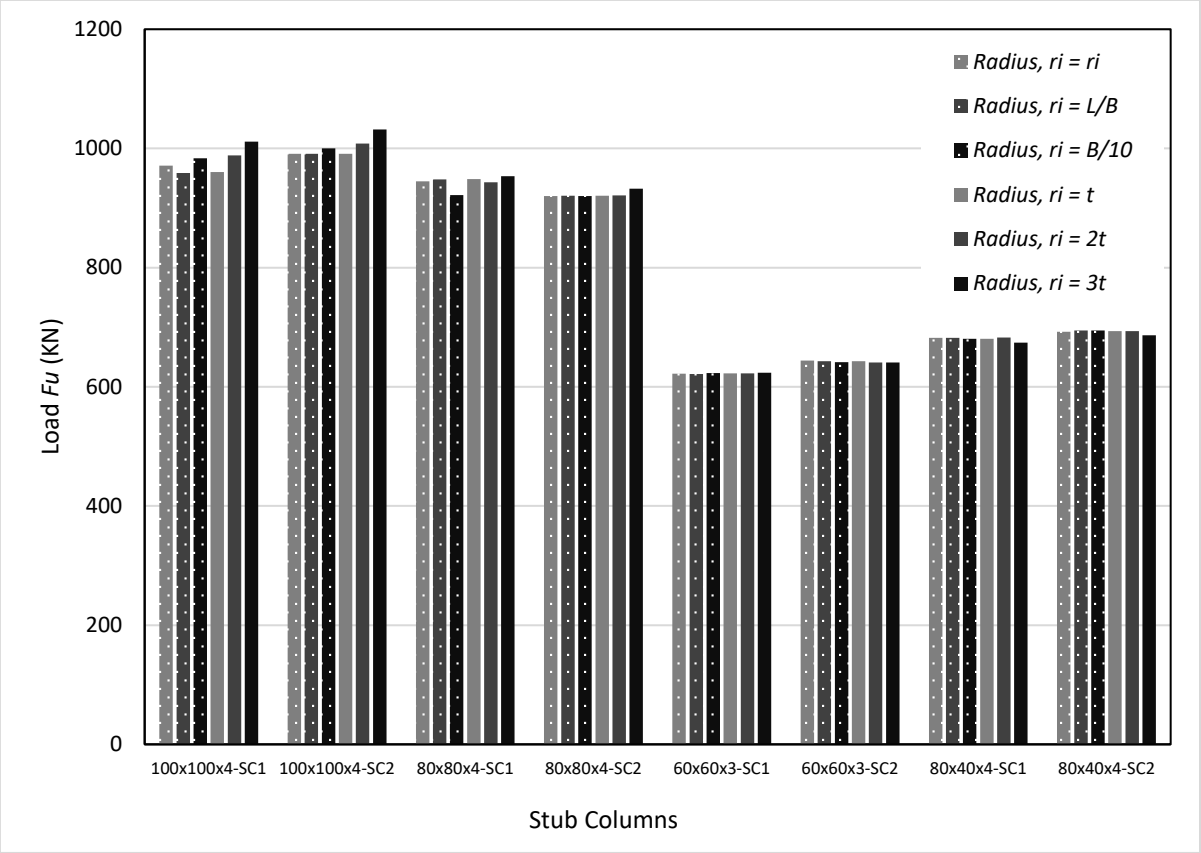

Figure 10 Different corner radius used in parametric study

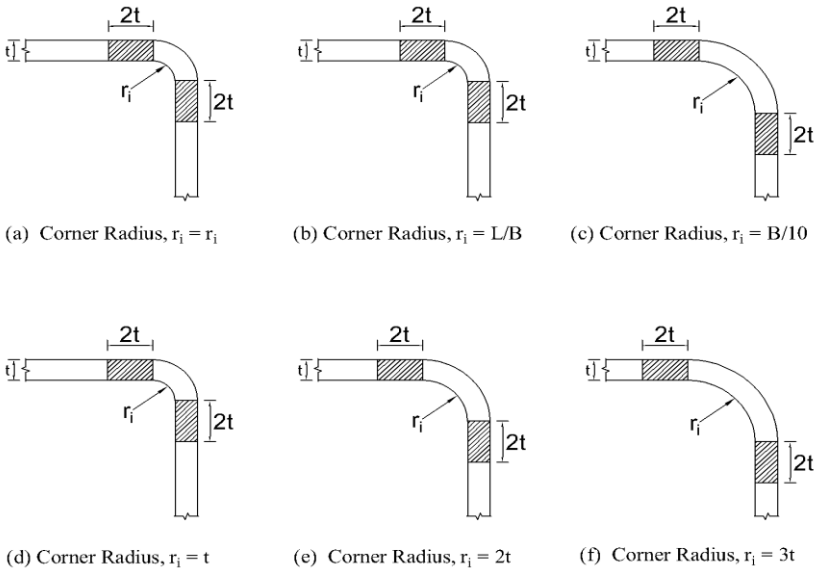

Figure 11 Maximum load carried by different columns at different corner radius

4.4 Load Eccentricity

In this study, two different hollow sections, namely square section and rectangular section, were taken. To illustrate the effects of load eccentricity properly, load eccentricity along both X & Y axis should be considered. However, since the square columns' dimensions along both X & Y axis is almost equal thus, their outcome would also be similar, so for square columns, only the eccentricity of load along the X-axis was considered. For rectangular columns, load eccentricity along both X & Y axis was considered.

For square columns, four different locations of load application were taken. The locations of load application were taken in such a way so that two of them fall inside the Kern zone ((1,0), (*B*/10,0)), one point at the edge of the Kern zone (*B*/6,0) and one point outside the Kern zone (*B*/4,0), where *B* is the least lateral dimension of the test specimen. Figure 12 shows cross-sections of different locations of load application for square columns and the results for square columns are presented in Table 10 and Figure 14.

For rectangular columns, a total of eight different locations of load application, four locations per axis, were taken. Along both X & Y axis, out of these four locations, two of them falls inside the Kern zone, one point at the edge of the Kern zone and one point outside the Kern zone; cross-sections of different locations of load application were shown in Figure13 and the outcomes of this parametric study for rectangular columns were shown in Table 11 & Figure 15.

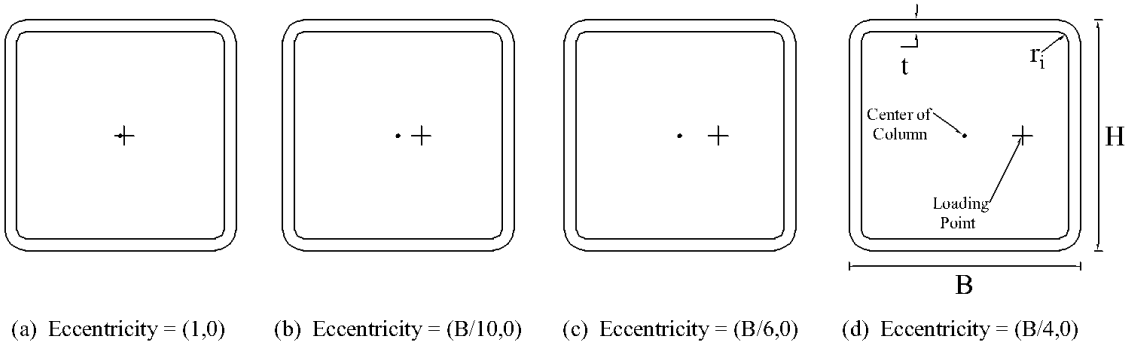

Figure 12 Eccentric Loading Points on the Column 60x60x3-SC1

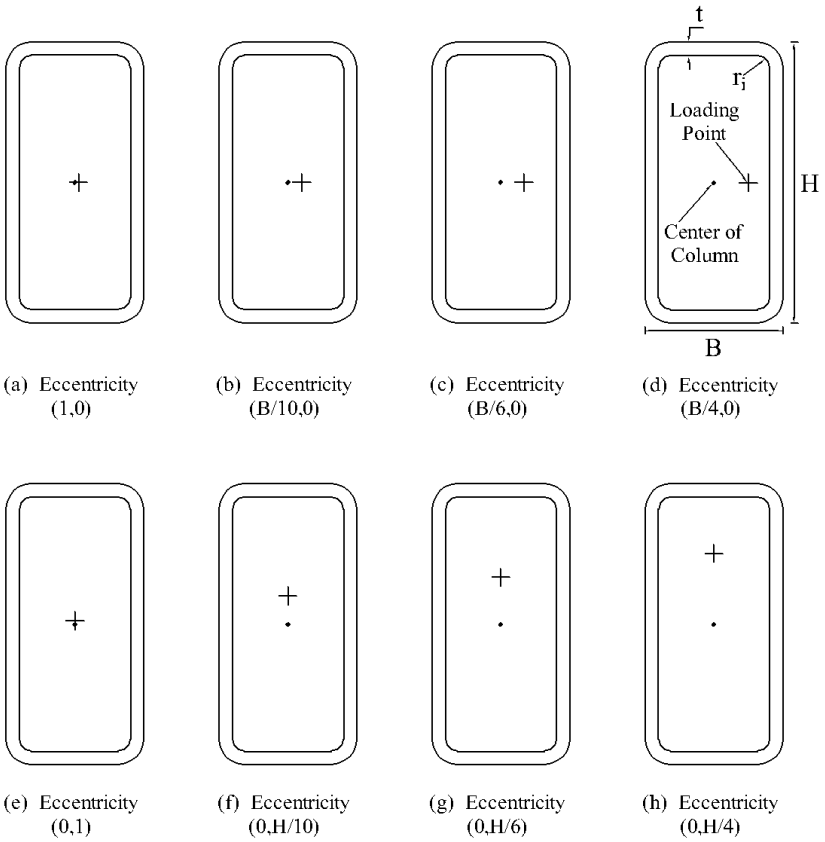

Figure 13 Eccentric Loading Points on the Column 80x40x4-SC1

Table 10 Findings of the parametric analysis of stub square columns under various eccentric loads in terms of load deformation

Designation	Test Results		Eccentricity = (1,0)		Eccentricity = (B/10,0)		Eccentricity = (B/6,0)		Eccentricity = (B/4,0)	
	F_u	d_U	F_u	d_U	F_u	d_U	F_u	d_U	F_u	d_U
	(KN)	(mm)	(KN)	(mm)	(KN)	(mm)	(KN)	(mm)	(KN)	(mm)
100x100x4-SC1	1022	3.63	971	2.71	874	2.29	784	1.98	697	1.96
100x100x4-SC2	1037	4.01	994	2.81	891	2.25	801	1.98	704	1.80
80x80x4-SC1	923	4.13	940	3.89	810	2.71	726	2.19	648	2.20
80x80x4-SC2	915	3.88	916	3.98	790	2.75	715	2.51	633	2.31
60x60x3-SC1	613	4.09	609	3.02	529	2.16	479	1.93	421	1.73
60x60x3-SC2	616	3.69	626	3.03	543	2.09	492	1.99	437	1.81

Table 11 Findings of the parametric study of stub rectangular columns under various eccentric loading in terms of load deformation

Designation	Along X-axis									
	Test Results		Eccentricity = (1,0)		Eccentricity = (*B*/10,0)		Eccentricity = (*B*/6,0)		Eccentricity = (*B*/4,0)	
	F_u	d_U	F_u	d_U	F_u	d_U	F_u	d_U	F_u	d_U
	(KN)	(mm)	(KN)	(mm)	(KN)	(mm)	(KN)	(mm)	(KN)	(mm)
80x40x4-SC1	709	4.33	631	2.451	559	1.914	454	1.803	670	3.511
80x40x4-SC2	710	4.12	646	2.543	572	1.910	470	1.901	681	3.236

Designation	Along Y-axis									
	Test Results		Eccentricity = (0,1)		Eccentricity = (0,*H*/10)		Eccentricity = (0,*H*/6)		Eccentricity = (0,*H*/10)	
	F_u	d_U	F_u	d_U	F_u	d_U	F_u	d_U	F_u	d_U
	(KN)	(mm)	(KN)	(mm)	(KN)	(mm)	(KN)	(mm)	(KN)	(mm)
80x40x4-SC1	709	4.33	534	1.891	448	1.954	523	2.168	461	1.962
80x40x4-SC2	710	4.12	546	1.794	458	2.061	532	2.152	471	2.052

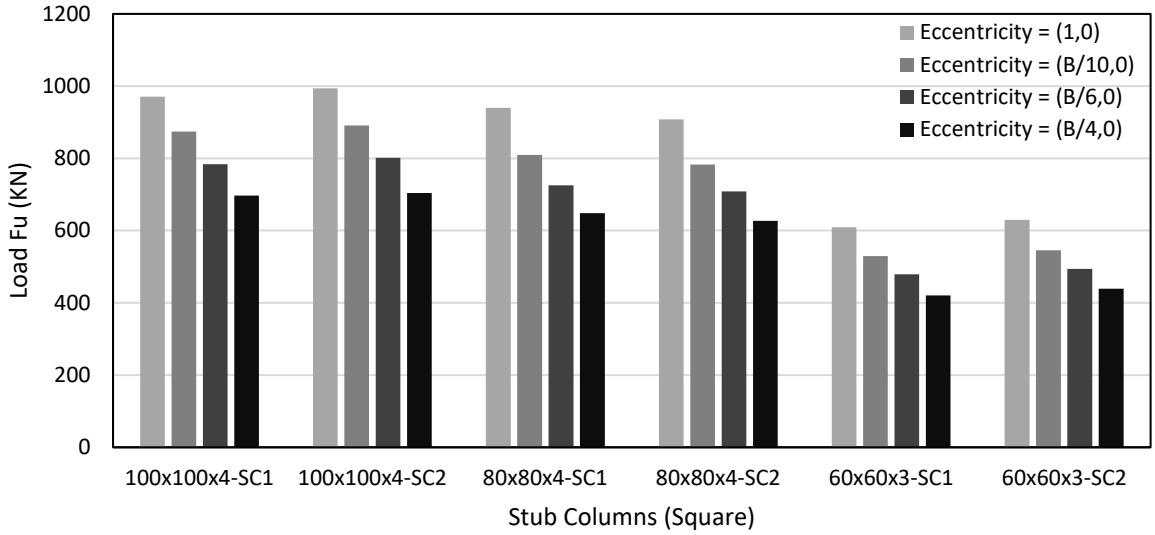

Figure 14 Maximum load carried by different columns (square) at different eccentricity

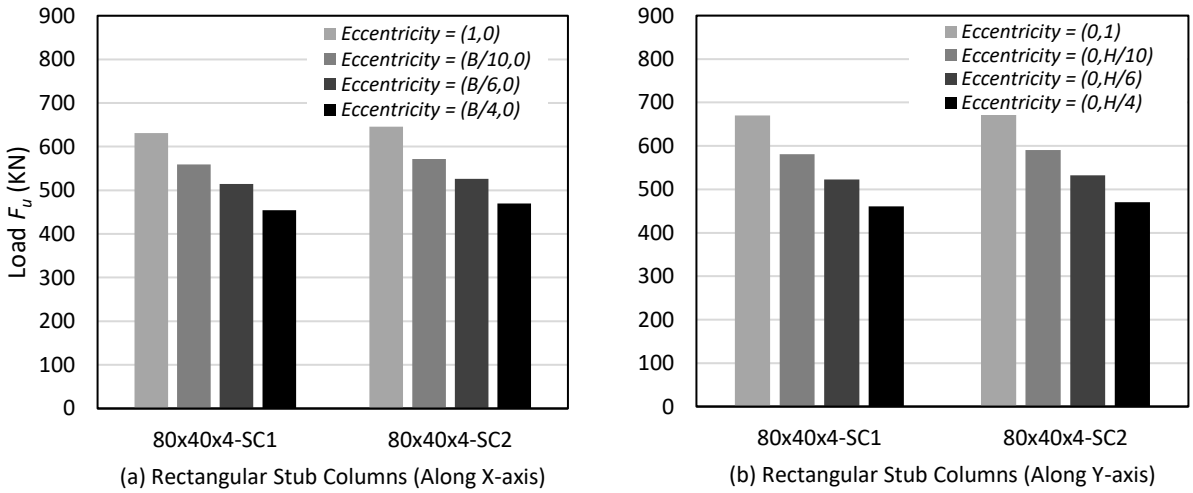

Figure 15 Maximum load carried by different columns (rectangle) at different eccentricities

4.5 Slenderness Ratio

The slenderness ratio is a crucial parameter for designing a column. The failure patterns of the column are primarily dependent on the slenderness ratio of the column. Five different lengths- 3*B*, 5*B*, 6*B*, 8*B*, and 10*B* were selected, other than the length of the test specimen, which is approximately 4*B*, where *B* is the least lateral dimension of the column. The column lengths were taken this way to avoid overall flexure buckling and thus keep the columns in a short column range. The outcomes of this parametric study are given in Table 12 and graphically in Figure 16 & Figure 17.

Table 12 Findings (Load & deformation) gathered from the Parametric Study of stub columns with various slenderness ratio

Designation	Test Results		Length, *L* = 3*B*		Length, *L* = 5*B*		Length, *L* = 6*B*		Length, *L* = 8*B*		Length, *L*= 10*B*	
	F_u	d_U	F_u	d_U	F_u	d_U	F_u	d_U	F_u	d_U	F_u	d_U
	(KN)	(mm)	(KN)	(mm)	(KN)	(mm)	(KN)	(mm)	(KN)	(mm)	(KN)	(mm)
100x100x4-SC1	1022	3.63	961	2.01	976	3.67	967	4.10	975	5.71	979	7.48
100x100x4-SC2	1037	4.01	1001	2.27	991	3.58	986	4.06	985	5.38	996	7.33
80x80x4-SC1	923	4.13	947	3.05	946	4.97	947	6.08	948	8.11	949	10.19
80x80x4-SC2	915	3.88	922	2.95	922	4.94	922	5.91	921	7.88	922	9.90
60x60x3-SC1	613	4.09	624	2.46	626	4.17	626	4.97	622	6.43	632	8.68
60x60x3-SC2	616	3.69	641	2.51	642	4.14	642	4.96	643	6.70	619	7.23
80x40x4-SC1	709	4.33	677	1.75	682	3.04	682	3.56	683	5.06	684	6.15
80x40x4-SC2	710	4.12	689	1.70	695	3.15	695	3.52	696	5.07	697	6.15

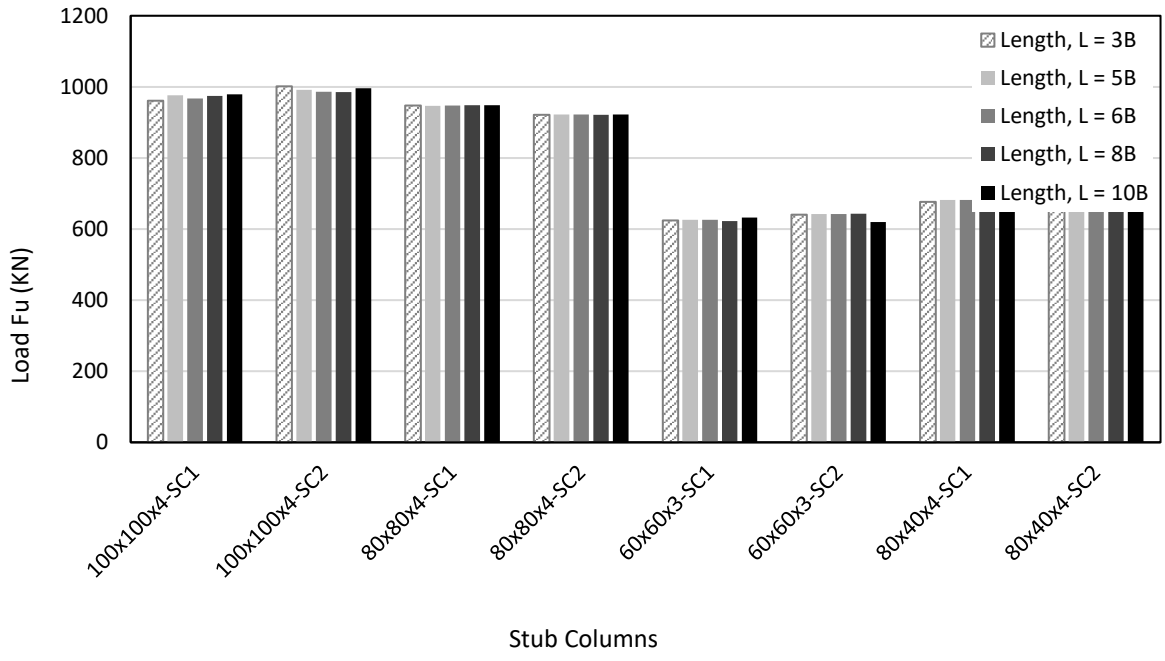

Figure 16 Maximum load carried by different columns at different slenderness

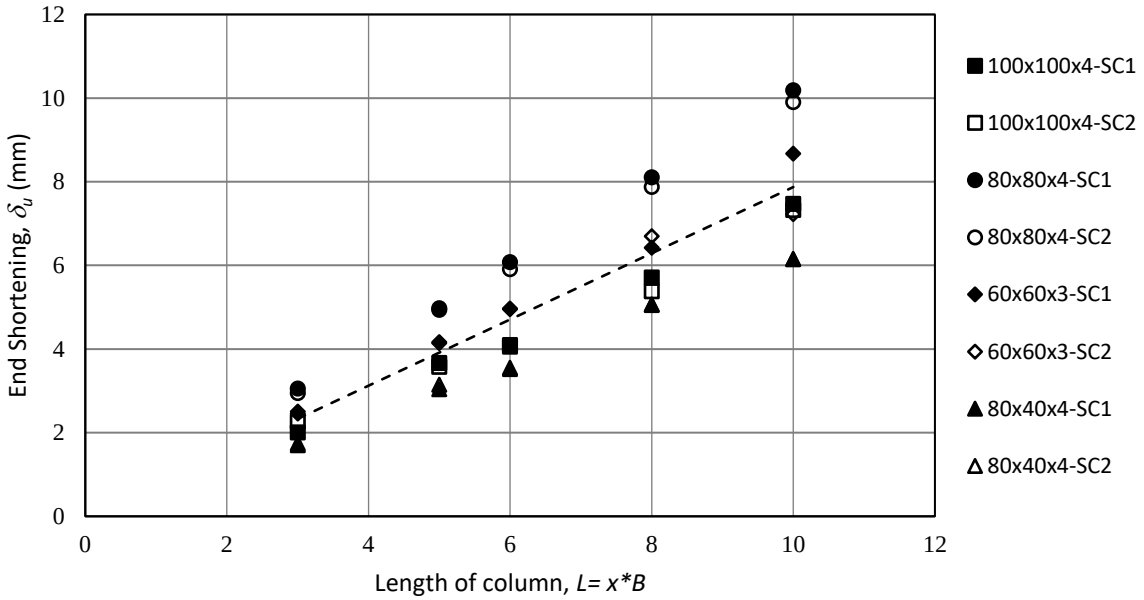

Figure 17 Stub columns with varying slenderness exhibit end shortening at maximum load.

5.0 RESULTS AND DISCUSSION

The parametric study was carried out to demonstrate how the various parameters affect the key design aspects of the studied material and section types. For this, a trendline of average values for each parameter was plotted, and a mathematical expression of the trendline was also determined. The outcomes of this parametric study are as follows.

5.1 Effect of the thickness (t)

The changes in the ultimate load and end shortening due to the changes in the cross-sectional area as a result of changes in thickness (t) is given in Table 8. Moreover, Figure 8 and Figure 9 graphically illustrate the variations in the ultimate load and corresponding end shortening for different thicknesses. Upon careful analysis of Table 8, it is evident that as the t increases, the F_u increases proportionally and all the column specimens follow the same trend. F_u increases about 30% on average with a 25% increase in t, and F_u increases to about 210% of the test results on average when t is doubled. However, F_u experiences a significant drop (about 70%) when t is decreased to half. This may be due to the instability of the column cross-section at the lower value of t [17]. Sachidananda et al. [17] observed similar findings for LDSS hollow stub columns with oval shapes, and Umbarkar et al. [32] also reported similar results for LDSS circular hollow columns with perforation. Both ultimate load and end shortening give linear trendlines and can be mathematically expressed as –

$$Fu = 988.77 * T - 209.08 \quad (5)$$

$$\delta u = 6.7653 * T - 3.4651 \quad (6)$$

Here, F_u the ultimate load

d_U stands for deformation under the maximum load

T is equal to x times the corresponding column's thickness (*t*)

x is any real number

5.2 Effect of corner radius

From the Table 9 and Figure 11, it can be clearly seen that the corner radius has no significant effects on ultimate load, with maximum variations of about 6% for SHS 10x100x4 column. Sachidananda et al. [17] reported that for oval shape, increasing the curvature of the flat region results in lower F_u. In our case, the possible reason behind observing no significant change in the F_u may be due to the fact that we only varied the corner radius, not the curvature of the fat region. For end shortening, columns SHS 100x100x4 and RHS 80x40x4 had considerable changes with about 30% and 20%, respectively, while for other columns the variation is insignificant.

5.3 Effect of Eccentricity

As the effects of load eccentricity along the X-axis and Y-axis would be identical for square sections, eccentricity was only studied along the X-axis. However, for rectangular sections, the eccentric load was applied along both axes to observe the variations due to differences in dimensions along the axes.
For each square column, ultimate load (F_u) as well as end shortening (d_U) show a linear decrease with the increase in eccentricity of load application. For eccentricity of (1,0), the variations in F_u are insignificant for all columns as the highest variation is for the SHS 100x100x4-SC1 column (5%). For load applied outside of the kern zone (B/4,0) F_u dropped by around 0% on average for all columns, while d_U dropped by almost 50% on average. With increasing F_u, all columns experienced early local buckling, which contributed to lower F_u and d_U. The relation between the ultimate load and distance of load application from the column center can be expressed mathematically in Equation (7) and Equation (8).

$$F_u = -992.52 * e + 835.51 \quad (7)$$

$$d_U = -2.5776 * e + 2.5335 \quad (8)$$

Here, F_u is the ultimate load
d_U stands for deformation under the maximum load
e is eccentricity or distance of load application from column center, expressed by $e = x*B$
x is any real number
B is the width of the column.

For rectangular columns, a similar trend to square columns can be seen. As expected, load carrying capacity of the columns differs when eccentricity is varied along two different axes. Columns show relatively higher load-carrying capacity for variation along the X-axis compared to the Y-axis.

5.4 Effect of Slenderness Ratio

From the results given in Table 12 and Figure 16, it can be conclusively seen that the slenderness ratio does not significantly affect the load-carrying capacity or the ultimate load. Column specimen 100x100x4-SC1 had the highest variation (6%), while 80x80x4-SC2 experienced almost no variation. Nonetheless, the slenderness ratio has a significant impact on d_U. For square columns, d_U doubled for most specimens, while for rectangular specimens, d_U increased by about 1.5 times. Figure17 shows the variation of d_U due to different column lengths, including a trendline with a positive slope. The mathematical expression for the trendline is given by Equation (10).

$$\delta u = 0.7916 * L - 0.0429 \quad (10)$$

Where, δu is the ultimate load
L (length of column) = $x*B$
x is any real number
B is the width of the column

6.0 CONCLUSION

Columns perform a vital role in transferring axial loads; therefore, a column's stress-strain behavior should be known before it is subjected to loading. This research performs a parametric study to see the effect of some key parameters like the thickness of the material, corner radius, load eccentricity and slenderness ratio on the ultimate load-carrying capacity and corresponding deformation. Numerical modeling was utilized for this purpose upon validating against experimental test results from the literature. Thickness & Eccentricity significantly affect both the load-carrying capacity and corresponding deformation, while the slenderness ratio only affects the deformation at the ultimate load. The corner radius shows no considerable effect on load-carrying capacity or deformation except for two specimens with a maximum variation of 30%. Columns identified as 100x100x4-SC1 and SC2 show slide variation in most cases compared to other specimens.
One of the limitations of this study is its focus on only four parameters for the parametric study. Studies on more parameters, such as curvature of flat region, load applied from jointing member, need to be done as they are also crucial for the column design. Although studies with different shapes of LDSS columns are available, there is still scope for further studies with different shapes and parameters. Moreover, the parametric study results could be compared with another Finite Element Modelling element.

Acknowledgement

The authors would like to thank everyone who helped us during this study. Also, the authors would like to thank the anonymous reviewers for their valuable comments and suggestions, which have significantly improved the quality of this manuscript.

References

[1] Francis, R. and G.J.M. Byrne, 2021. *Duplex stainless steels—alloys for the 21st century. . Metals.* 11(5): 836.
[2] Mirambell, E. and E. Real, 2000. *On the calculation of deflections in structural stainless steel beams: an experimental and numerical investigation. Journal of Constructional Steel Research,* 54(1): 109-133.
[3] Azad, S.K., D. Li, and B.J.J.o.C.S.R. Uy, 2020. *Axial slenderness limits for duplex and lean duplex stainless steel-concrete composite columns. Journal of Constructional Steel Research* 172: 106175.
[4] Kim, R., et al., 2021. *Hysteretic behavior comparison of austenitic and lean duplex stainless steel square hollow section members under cyclic axial loading. . Engineering Structures,* 237: 112227.
[5] Martins, A.D., R. Gonçalves, and D.J.E.S. Camotim, 2021. *Numerical simulation and design of stainless steel columns under fire conditions. . Engineering Structures* 229: 111628.
[6] Melo, J., et al., 2022. *Experimental and numerical investigation of the cyclic response of stainless steel reinforced concrete columns. Engineering Structures* 252: 113607.
[7] Ning, K., et al., 2021. *Experimental and numerical study of hot-rolled duplex stainless steel CHS columns. . Journal of Constructional Steel Research*180: 106579.
[8] Sachidananda, K. and K.D. Singh. *Numerical study of fixed ended Lean duplex stainless steel (LDSS) flat oval hollow stub column with square perforation under pure axial compression*. in *Structures*. 2021. Elsevier.
[9] Shu, G., et al., 2019 *Experimental and numerical study of cold-drawn duplex stainless steel square tube columns. Journal of Constructional Steel Research*. 156: 155-166.

[10] Singh, T.G. and K.D.J.T.-W.S. Singh, 2018. *Experimental investigation on performance of perforated cold–formed steel tubular stub columns.* Thin-Walled Structures,131: 107-121.
[11] Theofanous, M., T.M. Chan, and L.J.T.-W.S. Gardner, 2009. *Flexural behaviour of stainless steel oval hollow sections. Thin-Walled Structures* 47(6-7): 776-787.
[12] Theofanous, M. and L.J.E.S. Gardner, 2009. *Testing and numerical modelling of lean duplex stainless steel hollow section columns. Engineering Structures* 31(12): 3047-3058.
[13] Theofanous, M. and L.J.J.o.C.S.R. 2010. Gardner, *Experimental and numerical studies of lean duplex stainless steel beams Journal of Constructional Steel Research.* 66(6):. 816-825.
[14] Construction, A.I.o.S., *Steel construction manual*. 2005: American Institute of Steel Construction.
[15] Gardner, L. and D.J.J.o.C.S.R. Nethercot, 2004 *Experiments on stainless steel hollow sections—Part 1: Material and cross-sectional behaviour. Journal of Constructional Steel Research* . 60(9): 1291-1318.
[16] Liu, Y. and B.J.J.o.C.S.R. Young, 2003. *Buckling of stainless steel square hollow section compression members. Journal of Constructional Steel Research.* 59(2): 165-177.
[17] Sachidananda, K. and K.D.J.T.-w.s. Singh, 2015. *Numerical study of fixed ended lean duplex stainless steel (LDSS) flat oval hollow stub column under pure axial compression. . Thin-walled structures* 96: 105-119.
[18] Sachidananda, K. and K.D.J.T.-W.S. Singh, *Structural behaviour of fixed ended stocky Lean Duplex Stainless Steel (LDSS) flat oval hollow column under axial compression. Thin-walled structures* 2017. 113: p. 47-60.
[19] Theofanous, M., T.M. Chan, and L.J.E.s. Gardner, 2009. *Structural response of stainless steel oval hollow section compression members. . Engineering structures,* 31(4): 922-934.
[20] Gardner, L. and D.J.J.o.s.E. Nethercot, *Numerical modeling of stainless steel structural components—A consistent approach.* 2004. *Journal of structural Engineering,*130(10): 1586-1601.
[21] Ramberg, W. and W.R. Osgood, 1943. *Description of stress-strain curves by three parameters*. National Advisory Committee for Aeronautics Technical Note, No. NACA-TN-902,
[22] Gardner, L. and M.J.E.s. Ashraf, 2006. *Structural design for non-linear metallic materials. Engineering structures* 28(6): 926-934.
[23] Mirambell, E. and E.J.J.o.C.S.R. 2000. Real, *On the calculation of deflections in structural stainless steel beams: an experimental and numerical investigation. . Journal of Constructional Steel Research* 54(1): 109-133.
[24] Rasmussen, K.J.J.J.o.c.s.r., 2003. *Full-range stress–strain curves for stainless steel alloys. Journal of Constructional Steel Research* 59(1): 47-61.
[25] Ellobody, E. and B.J.J.o.C.S.R. Young, 2005. *Structural performance of cold-formed high strength stainless steel columns. Journal of Constructional Steel Research* 61(12): 1631-1649.
[26] Karren, K.W.J.J.o.t.S.D., 1967. *Corner properties of cold-formed steel shapes. . Journal of the Structural Division* 93(1): 401-432.
[27] Lecce, M. and K.J.J.J.o.S.E. Rasmussen, 2006. *Distortional buckling of cold-formed stainless steel sections: experimental investigation. Journal of Structural Engineering* 132(4): 497-504.
[28] Abdel-Rahman, N. and K.J.J.o.S.E. Sivakumaran, *Material properties models for analysis of cold-formed steel members. Journal of Structural Engineering* 1997. 123(9): p. 1135-1143.
[29] Riks, E., *The application of Newton's method to the problem of elastic stability.* 1972.
[30] Riks, E.J.I.j.o.s. 1979. *An incremental approach to the solution of snapping and buckling problems. International journal of solids structures* 15(7): p. 529-551.
[31] Chan, T.M. and L.J.E.s. Gardner, *Compressive resistance of hot-rolled elliptical hollow sections.* 2008. 30(2): p. 522-532.
[32] Umbarkar, K.R., L.M. Patton, and K.D.J.T.-W.S. Singh, 2013. *Effect of single circular perforation in lean duplex stainless steel (LDSS) hollow circular stub columns under pure axial compression. Thin-Walled Structures* 68: 18-25.